The Meteoritical Society

Meteoritics & Planetary Science 42, Nr 6, 935–949 (2007)
Abstract available online at http://meteoritics.org

Experimental shock decomposition of siderite and the origin of magnetite in Martian meteorite ALH 84001

M. S. BELL

Geosciences Department, The University of Houston, Houston, Texas 77204, USA
Jacobs Engineering, Johnson Space Center, Building 31, Room 222, Mail Code KT, Houston, Texas 77058, USA
Corresponding author. E-mail: mary.sue.bell1@jsc.nasa.gov

(Received 19 May 2006; revision accepted 25 January 2006)

Abstract–Shock recovery experiments to determine whether magnetite could be produced by the decomposition of iron-carbonate were initiated. Naturally occurring siderite was first characterized by a variety of techniques to be sure that the starting material did not contain detectable magnetite. Samples were shocked in tungsten-alloy holders (W = 90%, Ni = 6%, Cu = 4%) to further ensure that any iron phases in the shock products were contributed by the siderite rather than the sample holder. Each sample was shocked to a specific pressure between 30 to 49 GPa. Transformation of siderite to magnetite as characterized by TEM was found in the 49 GPa shock experiment. Compositions of most magnetites are >50% Fe^{+2} in the octahedral site of the inverse spinel structure. Magnetites produced in shock experiments display the same range of sizes (~50–100 nm), compositions (100% magnetite to 80% magnetite-20% magnesioferrite), and morphologies (equant, elongated, euhedral to subhedral) as magnetites synthesized by Golden et al. (2001) and as the magnetites in Martian meteorite Allan Hills (ALH) 84001. Fritz et al. (2005) previously concluded that ALH 84001 experienced ~32 GPa pressure and a resultant thermal pulse of ~100–110 °C. However, ALH 84001 contains evidence of local temperature excursions high enough to melt feldspar, pyroxene, and a silica-rich phase. This 49 GPa experiment demonstrates that magnetite can be produced by the shock decomposition of siderite as a result of local heating to > 470 °C. Therefore, magnetite in the rims of carbonates in Martian meteorite ALH 84001 could be a product of shock devolatilization of siderite as well.

INTRODUCTION

The debate about fossil life on Mars currently concentrates on magnetites of specific sizes and habits in the Fe-rich portions of carbonate concretions in Martian meteorite Allan Hills (ALH) 84001 (Golden et al. 2001; Thomas-Keprta et al. 2000). Golden et al. (2001) were able to demonstrate inorganic synthesis of these compositionally zoned concretions from aqueous solutions of variable ion-concentrations. They further demonstrated the formation of magnetite from siderite upon heating at 470 °C under a Mars-like, CO_2-rich atmosphere according to $3FeCO_3 = Fe_3O_4 + 2CO_2 + CO$ (French 1971) and they postulated that the carbonates in ALH 84001 were heated to these temperatures in an unspecified shock event. Devolatilization of the ALH 84001 carbonates would have occurred in a closed system or at least in the absence of free surfaces. Langenhorst et al. (2000) found bubbles or channels in ALH 84001 carbonates that they interpret to represent shock-induced degassing structures. Brearley (2003) described the presence of magnetite associated with voids in ALH 84001 carbonate which could be evidence of CO_2 loss. Barber and Scott (2006) describe "fine-grained carbonate that is partially decomposed to coarse-grained magnetite" in ALH 84001. A number of differential thermal analysis (DTA) studies of siderite (Bagin and Rybak 1970; Bell et al. 2000; Criado et al. 1988; Gallagher and Warne 1981; Lin et al. 2000; Pan 2000; Zakharov and Adonyi 1986) conclude that siderite decomposes at about 580 °C and the resultant FeO becomes oxidized to Fe_3O_4 in a CO_2 atmosphere at about 600 °C. Brearley (2003) describes the thermal decomposition relationships between end-member carbonates that represent the solid solution compositions found to comprise ALH 84001 carbonates. Observations based on experimental data (Harker and Tuttle 1955; Koziol and Newton 1995) show conclusively that siderite is much less stable than

© The Meteoritical Society, 2007. Printed in USA.

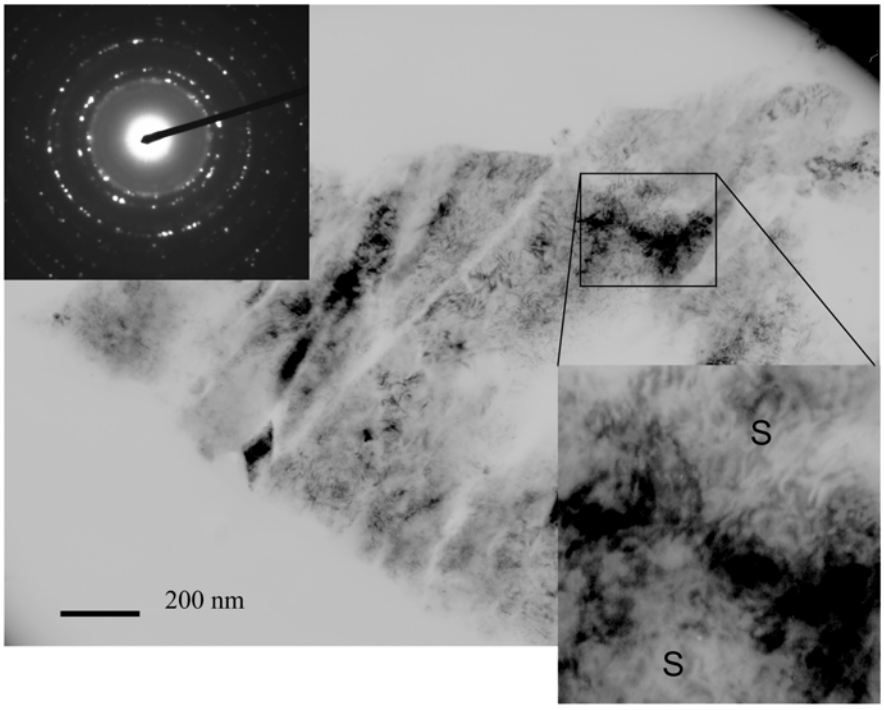

Fig. 1. TEM image of microtomed grain mount from 49 GPa shocked siderite experiment (Bell et al. 2002). Black areas are domains of nanophase spinel structure iron oxide within surviving iron carbonate identified by characteristic d-spacing in SAED pattern. Grouped spots in the SAED pattern are the manifestation of nanocrystalline spinels in non-random orientation. Enlargement shows the complex mottled contrast in siderite (S) due to extensively strained submicron domains where the crystal lattice is distorted.

rhodochrosite, magnesite, or calcite which are the three other significant solid solution components in carbonates in ALH 84001 (Brearley 2003).

The average shock pressure deduced for ALH 84001, substantially based on the refractive index of diaplectic feldspar glasses (Fritz et al. 2005; Stöffler 2000), is 32 GPa; associated temperatures increase by 100–110 °C. However, some of the feldspar, pyroxene, and a silica-rich phase was melted (Barber and Scott 2006; Bell et al. 1999; Mittlefehldt 1994; Schwandt et al. 1999a, 1999b; Shearer and Adock 1998) requiring local pressure deviations as high as 45–50 GPa. Langenhorst et al. (2000) report the carbonates in ALH 84001 to contain bubbles or channels that are interpreted to represent shock-induced degassing structures. They conclude from their observations that shock pressures must have been on the order of 50–60 GPa. Combining these shock studies with the above inorganic synthesis of zoned carbonates it would seem possible to produce the ALH 84001 magnetites by the shock-induced decomposition of siderite.

The extreme physical conditions of pressure, temperature, and strain imposed by transient shock waves during an impact event produce unique effects (e.g., mineral deformation, melting) in the rocks and mineral grains through which they pass. Although sediments, sedimentary rocks (including carbonates), water, and ice are major constituents of the outer crust of the Earth, most experimental and theoretical cratering studies have been directed toward volatile-free rocks. Whereas volatile-free rocks (such as quartz) may preserve unambiguous signatures of shock metamorphism, volatile-rich rocks such as carbonates may be completely vaporized. However, features caused by shock metamorphism may be preserved in rock textures or as new mineral phases. It is therefore possible that the magnetite in ALH 84001 could have been formed by shock devolatilization of siderite according to the equation from French (1971). This could explain the lack of siderite in the ALH 84001 zoned carbonate rims containing magnetite (McKay et al. 1996).

This hypothesis is tested here experimentally by exposing siderite to experimental shock. As reported earlier by Bell et al. (2002), intimately mixed zones of nanocrystalline spinel-structured Fe-Mg oxides were produced, based on preliminary transmission electron microscope (TEM) analyses and selected area electron diffraction (SAED) patterns (Fig. 1), in experimentally shocked siderite at 49 GPa. The magnetic components of this mix have now been concentrated by isolating magnetic grains from the bulk shocked material for chemical and other analyses of the shock products. Using a hand magnet drawn beneath weighing paper upon which the sample powder had been placed, magnetic particles were extracted from the bulk and subjected to dissolution using the techniques of Golden et al. (2001) for more detailed TEM identification and characterization of the shock products.

ANALYTICAL METHODS

Natural Copper Lake (Antigonish County, Nova Scotia, Canada) siderite was crushed, ground in alcohol and sieved to obtain the 120–250 μm size fraction. For the shock experiments, approximately 70 mg aliquots were encased in tungsten-alloy holders (W = 90%, Ni = 6%, Cu = 4%) to avoid any contribution of Fe from the sample holder to the reaction products. The experimental set up of the shock experiment is described by Gibbons et al. (1975) and Hörz (1970). Samples were shocked at pressures from 30 to 49 GPa in a CO_2 atmosphere (10^{-3} torr) to approximate conditions on Mars. Experiments were performed in the Johnson Space Center Experimental Impact Laboratory.

Powdered material was extracted and thermal gravimetric analysis of unshocked as well as shocked siderite samples was run on a TA Instruments model SDT 2960 Simultaneous DSC/TGA to determine CO_2 loss due to shock. Samples were heated from 25 °C to 900 °C at a rate of 10 °C/min in flowing nitrogen and weighed every 5 s to a sensitivity of 0.1 μg. The absolute weight loss determined by TGA upon complete outgassing represents the CO_2 that remained in the sample following shock; the difference between observed mass loss and that expected from ideally stoichiometric siderite thus represents the shock-induced CO_2 loss. TGA measurements consist of only one or two runs per shock pressure as the analysis consumes the sample.

Results of TGA were employed to choose the best candidate samples for examination by electron microprobe analysis (EMPA) and TEM. EMPA samples of unshocked siderite and untreated shocked siderite were mounted in epoxy, polished, and carbon-coated for analysis using the Johnson Space Center Cameca SX100 microprobe at an accelerating voltage of 15 kV, a current of 4 nA, and a peak count duration of 20 s, using wavelength dispersive spectrometers. Calibration was done using natural mineral and synthetic oxide standards. Backscattered electron (BSE) and elemental maps as well as quantitative analyses were acquired. Sample preparation for TEM involved two processes. In the first process, samples of powdered material were immersed in distilled water, sonicated for 5 s to disaggregate particles, and then floated onto carbon substrates on copper grids for examination. The other samples were treated with acetic acid to dissolve any remaining carbonate according to the methods of Golden et al. (2001), and then floated onto copper grids for examination. TEM bright-field, dark-field, and SAED patterns were acquired using a JEOL 2000FX STEM operating at 200 keV equipped with a NORAN System Six energy dispersive X-ray spectrometer (EDS) also at the Johnson Space Center. EDS spectra were collected with sufficient counts (5000) so that the uncertainty based on counting statistics was <3% for major elements. EDS detection limits are ~0.5 wt% for Fe, ~0.3 wt% for Mg, and ~0.1 wt% for S and Ca (Heinrich 1981). SAED patterns were indexed to identify phases present as the EDS beam size is too large to resolve individual objects in the 50–100 nm size range if they reside in a mixed component matrix. Bright field images reveal morphologies of the particles. The process of examining the 49 GPa shocked sample both untreated and treated with acetic acid was repeated three times to demonstrate reproducibility of the results. The total weight of sample used in the shock experiments was approximately 0.07 g per shot. Total harvested sample weights were approximately 0.05 g per shot.

SIDERITE STARTING MATERIAL

Siderite ($FeCO_3$) is an iron-bearing carbonate common to many diverse sedimentary settings, particularly in marine and lacustrine environments (Baker and Burns 1985; Ellwood et al. 1988; Ranganthan and Tye 1986) and in hydrothermal veins (French 1971). Substitution of Fe^{+2} by other metallic ions is common in siderite and the mineral is rarely found as pure $FeCO_3$. Both Mn and Mg commonly substitute for Fe^{+2} and there is complete solid solution between siderite and rhodochrosite and between siderite and magnesite (Deer et al. 1997). Thermal decomposition and oxidation of the mineral siderite is of interest because siderite represents an ore of iron (Bagin and Rybak 1970; Criado et al. 1988; French 1971; Gallagher and Warne 1981; Zakharov and Adonyi 1986). The initial decomposition temperature is dependent on substitution of Mn^{+2} and Mg^{+2} for Fe^{+2} but even a few percent MnO or MgO is not enough to noticeably increase the temperature (Kulp et al. 1951).

In hand specimen, the siderite appears coarse-grained with crystals ranging from 5–10 mm in size and it contains veins or coatings of alteration minerals in fractures and voids. Quantitative EMP analysis taken in 1 μm steps across representative grains mounted and polished in epoxy determined the siderite starting material to vary from 7.0–20.9% $MgCO_3$, 67.4–79.2% $FeCO_3$, 11.4–13.7% $CaCO_3$ with trace amounts of Mn, Cr, and S (Table 1). Analysis totals are from 2.11 to 4.96% low due to the difficulty in obtaining a well-polished surface and the volatile nature of the iron carbonate material.

Several analytical techniques were used to characterize the iron phases in the starting material and to ensure that no detectable magnetite was present prior to shock. Iron sulfides and trace amounts of Mn and Cr were identified by energy dispersive spectroscopy (EDS). Representative backscatter electron image surveys of unshocked polished grains show the relative abundance of iron sulfides to be variable. Some siderite grains are free of iron sulfide. Some iron sulfide grains are as much as a micron in size (Fig. 2). Elemental maps of Mg, C, Ca, Fe, Si, S, Cr, and O were used to characterize the siderite. The BSE image and Mg and Fe maps in Fig. 3 reveal Mg-rich domains within the iron carbonate.

Table 1. EMP quantitative analysis of unshocked siderite, the starting material for the experiments. Trace Mn was detected in analysis 4. Cr and S were detected in trace amounts in analyses 3 and 8. See text for instrument conditions.

	1	2	3	4	5	6	7	8	9	10	11
1 cation											
Fe	0.674	0.676	0.681	0.687	0.676	0.675	0.677	0.677	0.675	0.675	0.792
Mg	0.206	0.207	0.202	0.197	0.206	0.207	0.206	0.207	0.209	0.208	0.070
Ca	0.120	0.118	0.114	0.117	0.118	0.118	0.117	0.116	0.117	0.117	0.137
weight%											
FeO	46.10	45.38	45.70	46.02	44.93	45.34	45.77	45.09	45.24	44.83	45.13
MgO	14.12	13.88	13.56	13.19	13.68	13.91	13.92	13.79	13.98	13.84	4.01
CaO	8.19	7.91	7.84	7.81	7.85	7.96	7.89	7.72	7.83	7.76	7.81
CO_2	29.44	28.57	28.00	28.71	28.90	28.83	28.30	28.39	28.76	28.65	28.87
Totals	97.85	95.73	95.11	95.72	95.35	96.03	95.89	95.00	95.80	95.09	95.83

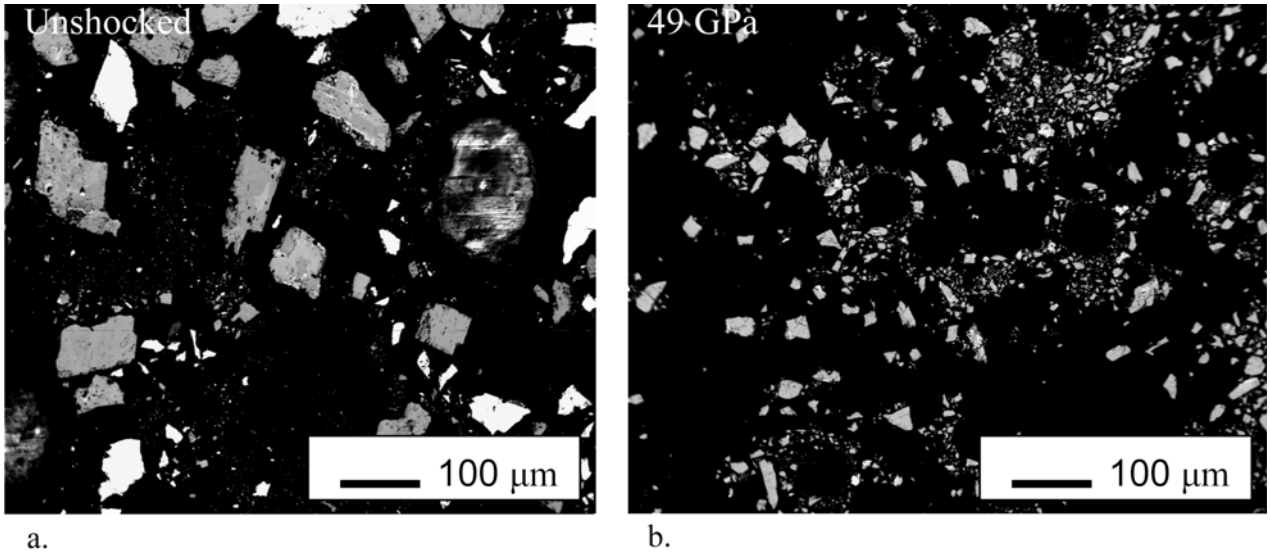

Fig. 2. Backscattered electron (BSE) images representative of (a) unshocked siderite grain mount and (b) 49 GPa shocked grain mount. Scale is the same for both images. White grains are iron sulfides and gray grains are porous siderite. Grain size has been significantly diminished by the shock experiments to <50 μm.

These maps also reveal the porous nature of the polished grain surfaces. Localized iron enrichments occur in fractures where silica-rich alteration products and iron sulfides occur (Fig. 3, Fe map). However, Mg does not correlate with local iron enrichments in unshocked grains (Fig. 3, Mg map). The presence of iron sulfides and other alteration minerals as evidenced in the iron, silica, and sulfur maps in Fig. 4 is consistent with compositions in published reports of natural siderite (see above references). Magnetic susceptibility of this natural siderite is ~8×10^{-7} m^3/kg (mid-range for published values, 4–12×10^{-7} m^3/kg). This corresponds to <1.6 ppt of some possible combination of paramagnetic, ferromagnetic, and/or diamagnetic minerals in the starting material and is three orders of magnitude less than values for crustal rocks with low magnetic susceptibility (Telford et al. 1976). Mössbauer spectroscopy was used to analyze a powdered sample of the starting material. No magnetite was detected as determined from the ^{57}Fe Mössbauer spectra (to a detection limit of 0.5%). A powdered sample of unshocked siderite was dissolved in acetic acid according to the methods of Golden et al. (2001) (soaked in a 20% acetic acid bath at 65 °C for 72 h) and the residue was examined by TEM to further characterize the material used for these shock experiments. The iron-bearing phase in the residue from the dissolved unshocked siderite is hematite. No spinel-structured iron oxides were identified in the siderite starting material.

RESULTS OF SHOCK EXPERIMENTS

Cursory examination of the experimentally shocked siderite indicates alteration of the starting material (Fig. 5). The natural, unshocked siderite is reddish in color, but all shocked samples have been transformed to gray that grades to black with increasing shock pressure. Magnetic particles can readily be separated from the powdered material shocked to pressures >39 GPa with a hand magnet. This was not evident in the samples shocked to lower pressures. Initial results of TGA are not systematic. Mass loss does occur with increasing

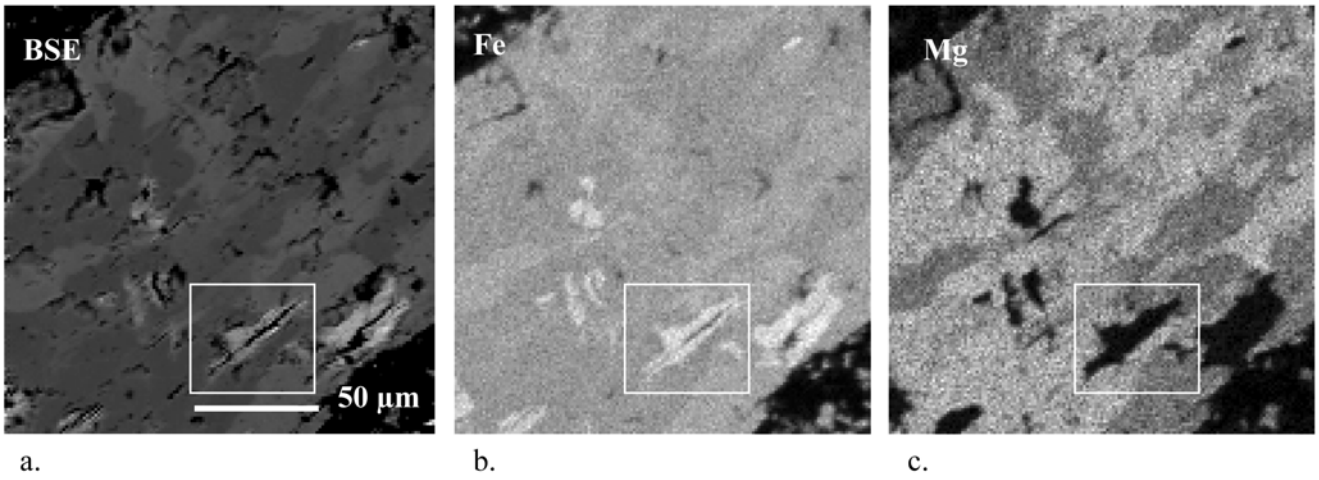

Fig. 3. EMPA backscattered and elemental maps of an unshocked siderite grain showing typical distribution of iron and magnesium-rich domains. a) The BSE image illustrates the porous nature of the grain surfaces. Note Fe enrichments associated with voids contain no Mg (b and c). All three images are the same area of the same grain.

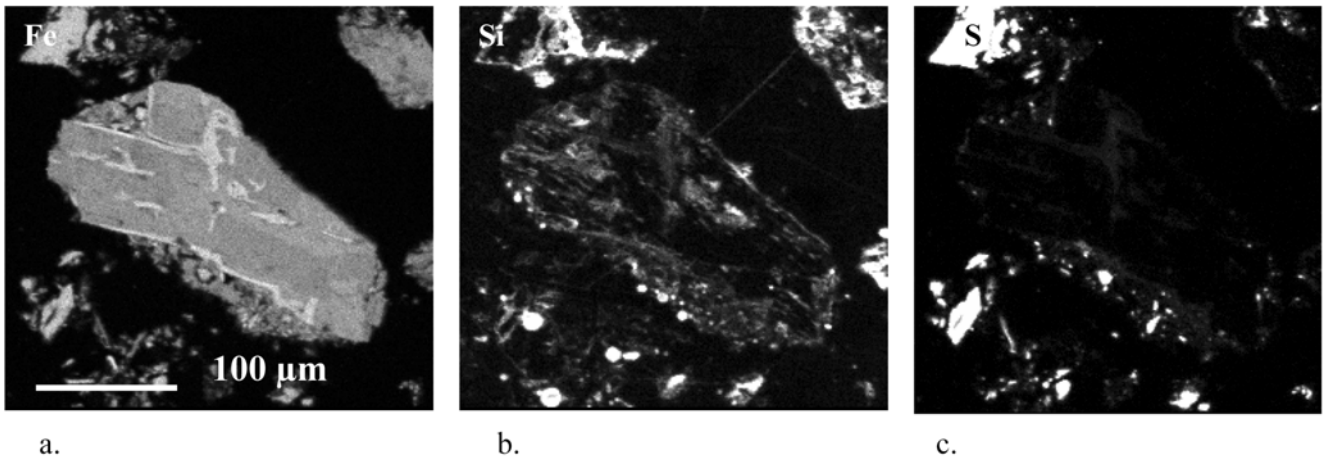

Fig. 4. Electron microprobe elemental maps of a representative unshocked siderite grain. a) Localized iron enrichments occur along microfractures and are probably hematite that was found in the residue after dissolution of the carbonate (b). A silica-rich phase, probably alteration of the siderite, is located in some of the same fractures as iron (c). Sulfur map shows the presence of iron sulfides in the starting material. Chromium was analyzed for, but not detected. All three images are the same siderite grain.

shock pressure, but the 24.8 GPa experiment shows no appreciable mass loss (Fig. 6). However, the 30.2 GPa sample has the greatest mass loss, whereas the sample shocked to the highest pressure (49 GPa) has one of lowest mass losses. After re-running TGA on new aliquots of two samples, the 30.2 GPa sample resulted in a similar mass loss as the original run. However, the 49 GPa sample resulted in an increased mass loss more in line with the expected trend of increasing mass loss with increasing shock pressure. The highest pressure experiment was chosen for further examination under the assumption that its shock effects were greatest, based on its color change from red-orange to black as well as the ease of extracting enough magnetic particles for TEM analysis from the recovered material compared to the lower pressure shock experiments.

EMP maps and BSE images show that grains in the 49 GPa sample are smaller in size than those of the starting powder and that the abundance of large iron sulfide grains is reduced (Fig. 2). Shocked siderite grains are highly fractured, some along cleavage planes, but also in irregular patterns (Fig. 6). Shocked siderite grains retain the porous surface appearance of unshocked grains. Iron and magnesium enrichments correlate in veins and pockets although Fe >> Mg and areas of iron concentrations free of Mg can be seen in Fig. 6. Compositional boundaries between Fe and Mg-enrichments and surrounding siderite are sharp (Fig. 6). Carbon blebs <10 μm in size were detected in cracks and veins where iron is also concentrated (Fig. 6d). Chromium and sulfur were not detected in many shocked grains although iron sulfide blebs can be found preserved in

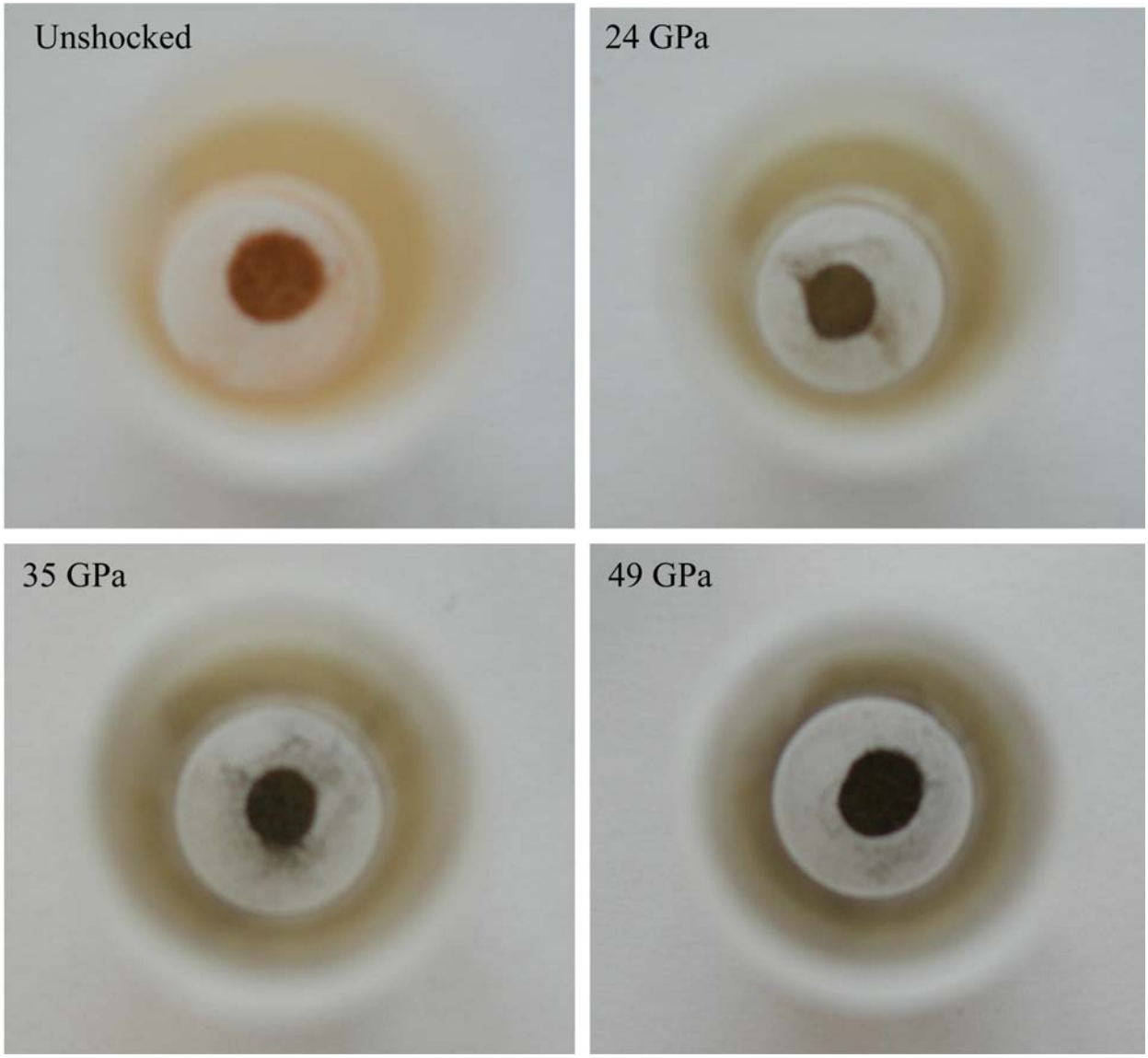

Fig. 5. Unshocked and shocked siderite powders photographed in vials. The unshocked sample of starting material is reddish in color. Shocked samples progressively changed in color with increasing shock pressure from dark gray to black.

veinlets within remaining siderite grains. Textures indicative of melt (irregular blebs, globules, embayments, vessiculation, flow and spinifex textures) observed in shocked carbonate from the Haughton impact structure (Osinski and Spray 2001) were not observed in siderite grains shocked to 49 GPa. Some carbonate remains intact in all shocked siderite grains examined as evidenced by the EMP elemental maps.

Figures 8–14 show TEM images of shocked siderite from the 49 GPa experiment. Interiors of residual carbonates in untreated samples contain extensive regions hundreds of nanometers in size of electron-dense crystals in the ~50–100 nm size range. These crystals occur in clusters within and on margins of remaining siderite (Fig. 7). Diffuse and weakly streaked diffraction spots in SAED patterns of untreated samples as well as d-spacings (lattice spacings) characteristic of both siderite and another phase indicate a mixture of many non-randomly oriented crystallites (Fig. 8a). However, SAED patterns acquired on grain margins are characteristic of a single phase and are a good fit to solid solution spinel (Figs. 8b and 9). Many magnetites in the <50 to 100 nm size range possess both equant and elongated forms (Fig. 10 at arrows). Some grains have euhedral forms but most do not. Elongated euhedral magnetite crystals can be seen in Figs. 10 and 11. The two largest crystals in Fig. 11 are either intimately intergrown or are magnetically attracted to each other. These magnetite crystals lack microstructure, suggesting they nucleated in the shock experiment, whereas the residual siderite has mottled contrast from lattice strain acquired during shock.

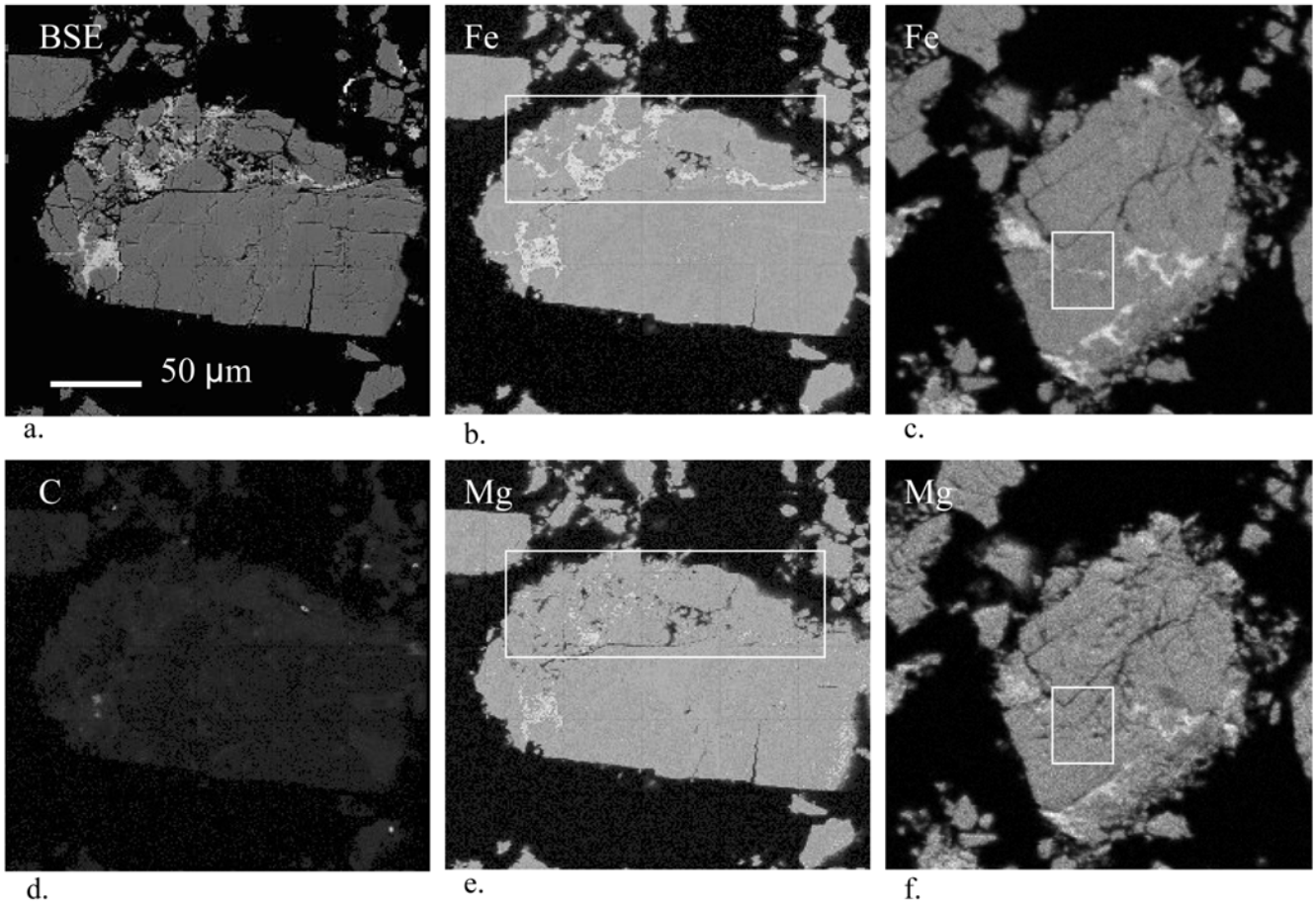

Fig. 6. EMP elemental maps of typical siderite grains shocked to 49 GPa. a) Fractures in the lower right half of the grain follow cleavage patterns but are more irregular in the upper left portion of the grain. Localized iron (b and c) and magnesium (e and f) enrichments are detected in portions of these grains, but Mg is not always associated with Fe enrichments (boxes) and may indicate the presence of periclase. Carbon can be detected above background (d). Scale is the same for all images.

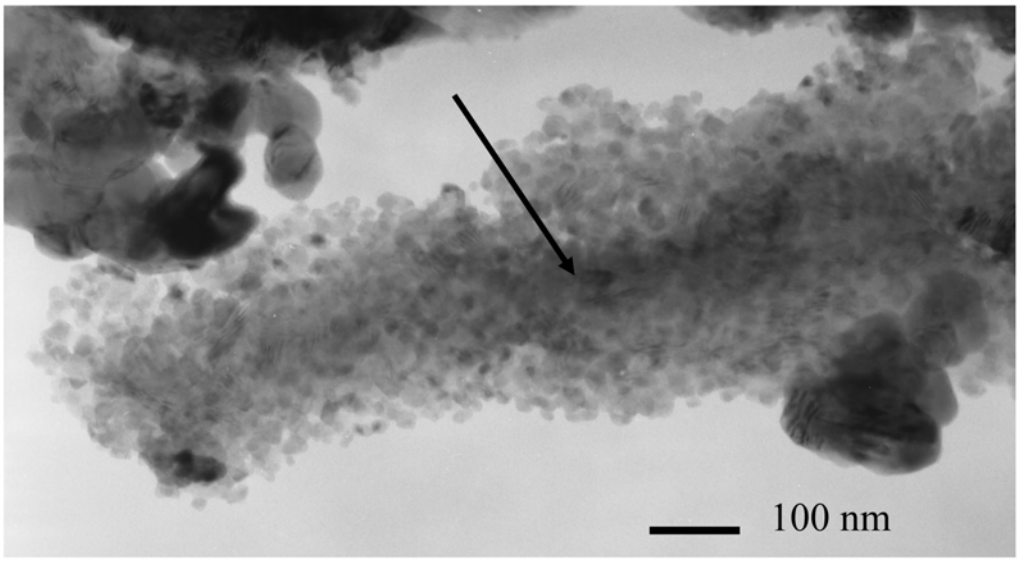

Fig. 7. TEM bright-field image of untreated magnetite. Interior of residual carbonate (arrow) contains electron-dense regions of nucleating magnetite in the <100 nm size range.

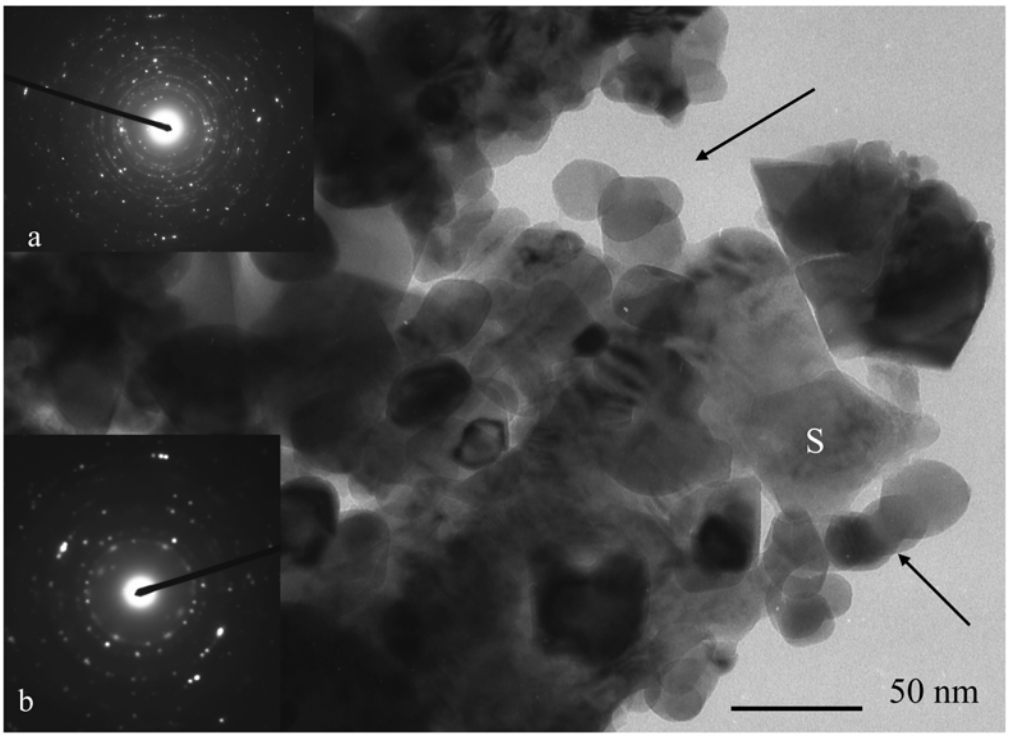

Fig. 8. TEM bright-field image of untreated shocked siderite sample. SAED pattern (a) from the imaged area is characteristic of a mixture of siderite (S) and magnetite crystals. The mottled contrast of strained siderite is in marked contrast to the defect free contrast of the magnetite crystals (at arrows). The offset diffraction spots in SAED pattern (b) are indicative of several magnetite crystallites in slightly preferred orientation. Arrows point to <50 nm, equant, euhedral to anhedral magnetite crystals.

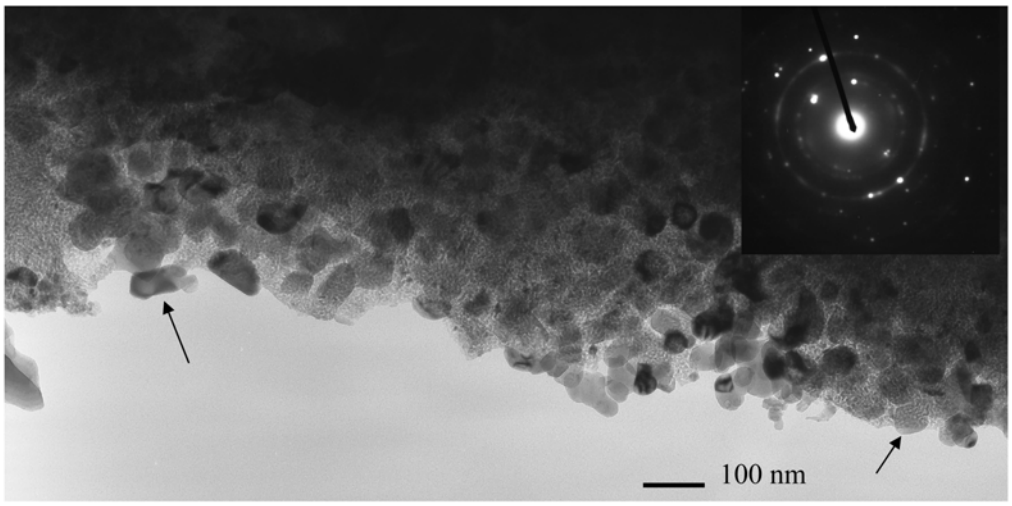

Fig. 9. TEM bright-field image of untreated magnetite on the margin of residual siderite. Equant and elongated magnetites, some euhedral, are visible at arrows. SAED pattern is characteristic of magnetite.

Acid-treated samples shocked to 49 GPa contain the same sizes and morphologies of shock-produced magnetite crystals as the untreated samples. However, the SAED patterns of samples treated to remove siderite are characteristic of one phase and lack the characteristic d-spacings of siderite (Figs. 12 and 13). TEM examination of the shock-produced crystals before and after the acetic acid treatments indicates that the acid extraction did not alter the size, shape, or surface textures of the shock-produced crystals.

EDS analyses of shock-produced oxides result in a range of compositions (Fig. 14). Fe_{tot} ranges from 80.69–100% of total cations in the nucleating phase; the other major cation detected in some single crystals is Mg. Crystals of all shapes

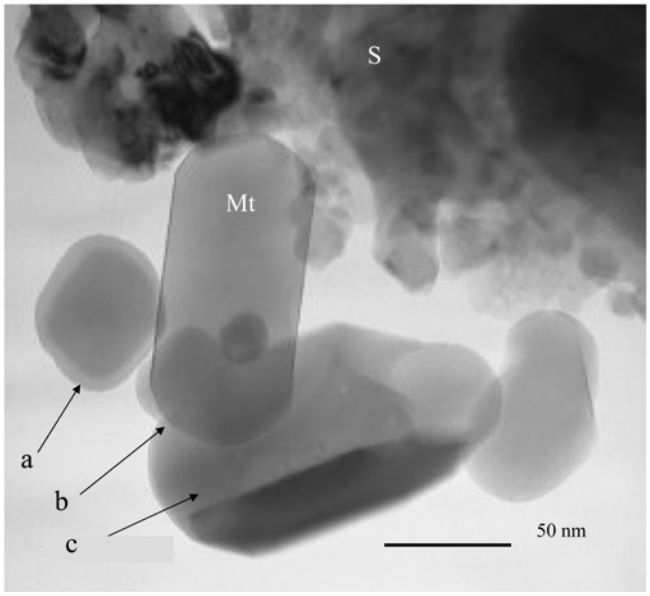

Fig. 10. TEM bright-field image of untreated magnetite. To the upper right is siderite (S) containing nucleating crystallites of magnetite. a) equant, b) euhedral elongated, and c) subhedral elongated magnetite crystals are in the lower left of the micrograph.

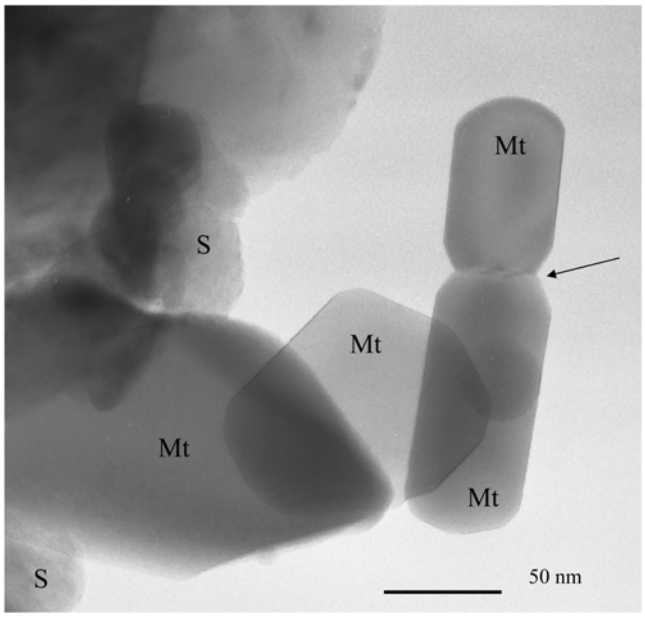

Fig. 11. TEM bright-field image of untreated magnetite produced in the experiments. Magnetite crystals (Mt) on edge of residual siderite (S) display defect free contrast. Elongated euhedral magnetite grains at right appear to be intergrown (at arrow).

and sizes have the same range of compositions. Trace amounts of Si, Ca, Mn, Cr, and S can be detected in dense areas of untreated samples where multiple phases are indicated by SAED patterns.

DISCUSSION OF SHOCK EXPERIMENTS

After shock, the color change of the siderite suggests that a systematic alteration effect has occurred on the macroscale, but microanalysis reveals the alteration to be incomplete. Intact siderite is present in EMP maps of shocked grains. Iron and magnesium enrichments are present in highly fractured zones (Fig. 6). Residual iron carbonate mixed with crystals of another iron-rich phase is detectable in SAED patterns from TEM examination of both acid-treated and untreated shocked samples (Fig. 8). However, SAED patterns acquired from electron-dense crystals on the margins of residual iron carbonate indicate the presence of only a single phase.

Table 2 compares d-spacings measured from SAED patterns of the shocked crystals with published d-spacings for magnetite and magnesioferrite (Joint Committee for Powder Diffraction 1980). Even within a measurement uncertainty of ~1%, the SAED patterns for magnetite, magnesioferrite, and these shock products are indistinguishable (Brearley 2003).

EDS measurements of the shocked crystals detected Fe in concentrations >80% of the total cation concentration. Figure 14 is a histogram of seven EDS measurements taken from a variety of spinel morphologies found within and at margins of remaining siderite. These analyses represent the range of compositions in shock-produced spinels. A horizontal line at 83% represents the dividing line between <50% Fe^{+2} and >50% Fe^{+2} in the octahedral site of the spinel structure. EDS analyses of the spinels produced in these shock experiments show that most contain >50% Fe^{+2} and Mg is not detected in some measurements. Magnetite and magnesioferrite are isostructural Fd3m inverse spinels of the magnetite series solid solution (Deer et al. 1997). For solid solutions, the "50% rule" applies (Nickel 1992; Nickel and Grice 1998). A complete solid solution series without structural order of the ions defining the end members is arbitrarily divided at 50 mol% and the two portions are given different names. To indicate a significant (but minor) amount of Mg, for instance, a Schaller adjective modifier may be assigned such as magnesian magnetite (Schaller 1930). For magnetite, the 50% rule applies to the Fe^{+2} cation site (octahedral site). Therefore, most spinels analyzed here by EDS are magnesian magnetite and some are "pure" magnetite.

The only published data on the compositional purity of ALH 84001 magnetites, one of the five criteria for biogenicity following Thomas-Keprta et al. (2000), can be found in Thomas-Keprta et al. (2000). All subsequent publications (Thomas-Keprta et al. 2001; Thomas-Keprta et al. 2002) refer to these data. Brearley (2003) states "the experimental conditions for other spectra reported by Thomas-Keprta et al. (2000) are somewhat different from those of the standard spectra" and that "these data cannot be used to argue unequivocally for or against the presence of minor or trace concentrations of Mg, Al, etc. in the elongated prismatic magnetites from ALH 84001." (See Brearley [2003] for further discussion of chemically pure magnetite in ALH

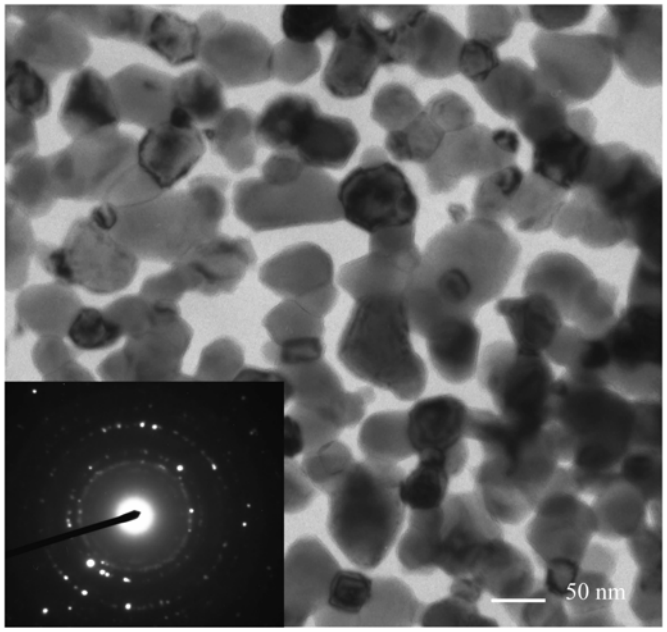

Fig. 12. TEM bright-field image of acid-treated magnetite. Most residual siderite has been removed by etching and magnetite remains. SAED pattern is characteristic of magnetite crystals. The same range of morphologies (euhedral, subhedral, anhedral, equant, and elongated) can be found in the treated shock sample an in the untreated sample.

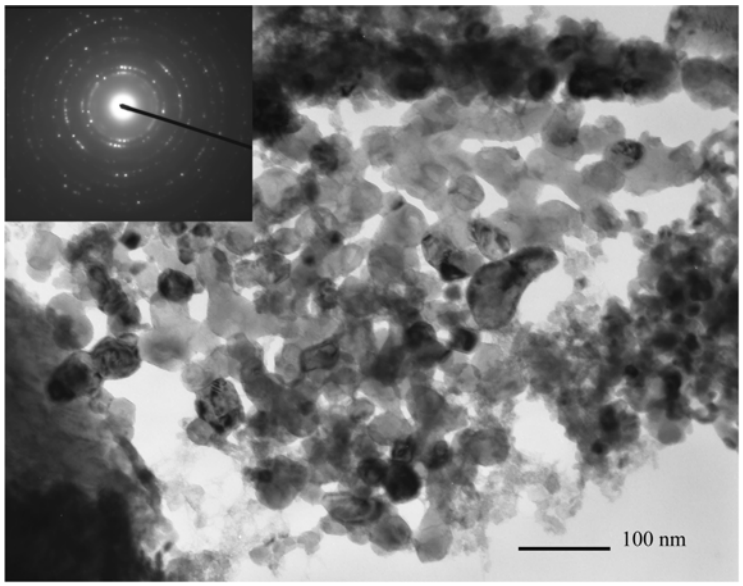

Fig. 13. TEM bright-field image of acid-treated shock product and SAED pattern characteristic of magnetite. Image contains equant, euhedral, and anhedral randomly oriented magnetite crystals in the <100 nm size range.

84001). ALH 84001 magnetite was extracted by Golden et al. (2006), and analyzed using the same instrument as Thomas-Keprta et al. (2000) and this study. Golden et al. (2006) found ALH 84001 magnetites to contain from 3.0 mol% Mg to an amount below detection after acquiring 5000 counts. Magnetite created in this study ranges from "pure" Fe_3O_4 (Mg not detected in EDS) to compositions containing 19.31 mol% Mg. These amounts closely reflect compositions of the siderite starting material for the shock experiments which was composed of local areas with iron concentrations and no associated Mg to as much as 20.9 mol% $MgCO_3$. Comparatively, magnetite-bearing carbonate layers in ALH 84001 have compositions from ~10% $MgCO_3$ to ~60% $MgCO_3$ (Treiman 2003). Golden et al. (2006) have shown that magnetite created by heating Mg-rich siderite + pyrite to 350 °C in a closed system and kept at set temperature for approximately nine days was compositionally indistinguishable from magnetite in ALH 84001.

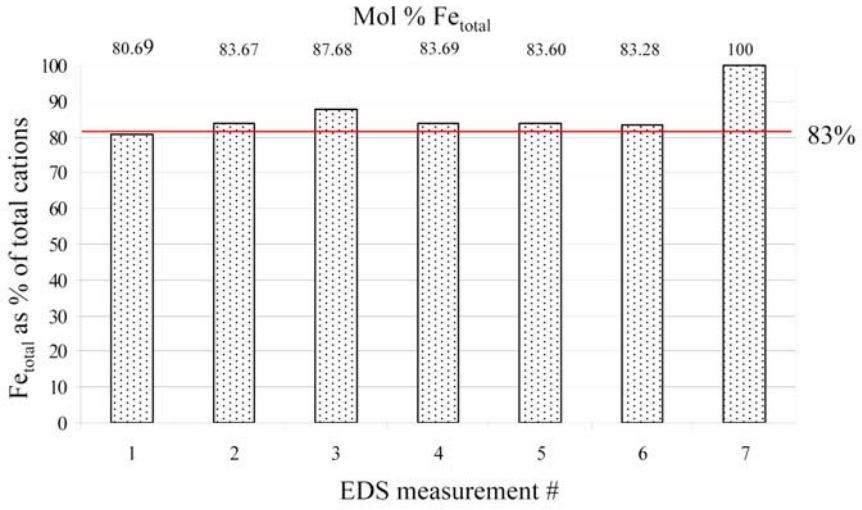

Fig. 14. Histogram of EDS measurements for iron as a percent of the total cations in the shock-produced spinels. Compositions with >83 mol% Fe_{total} have >50% Fe^{II} in the spinel structure (magnetite composition). With the exception of analysis 1, these shock products are magnetite. Mg is the only other major cation detected in these magnetite crystals.

The starting material for these shock experiments does contain iron sulfides. However, the duration of the localized temperature excursion in these shock experiments is short (less than 100 μs). This short time scale precludes large-scale cation diffusion and mitigates any effect of fO_2 created by the presence of iron sulfides in the siderite, thereby allowing the inclusion of Mg, if present locally, into the magnetite structure. However, the decomposition experiments of Brearley (1986) demonstrate that under disequilibrium conditions, the earliest phase that forms from mixed component phases is a simple binary oxide rather than a more complex solid solution because it is kinetically the easiest to nucleate. Formation of magnetite by shock experiment is a disequilibrium process that results in rapid heating and cooling of the shocked material. The earliest stages of incipient decomposition produce many small nucleating crystals as observed.

The bulk of the iron carbonate is not completely devolatilized in the 49 GPa shock experiment. The spatial relationships of magnesium to iron in the shock experiment at 49 GPa is similar to that before the experiment. Shocked siderite grains from these experiments show no compositional gradients in EMP elemental maps which would indicate diffusion of cations from the siderite-composition domains towards iron enrichments. Magnetite crystals from the shock experiments may be produced at the expense of iron-rich phases concentrated in alteration zones (fractures and voids) or in more end-member like iron-rich siderite domains in the natural siderite (or both) as iron carbonate compositions are the first to thermally decompose. In the case of pure $FeCO_3$ domains, the spinel shock product would be pure magnetite. Magnesium detected by EDS in the spinel-bearing material may be present in the spinel structure, in residual siderite, or represent a separate oxide phase such as periclase, but has yet to be resolved (the 400 and 440 diffraction rings for magnetite occur at nearly the same position as the 200 and 220 rings for periclase). Barber and Scott (2002) report occurrences of nanocrystalline periclase associated with Mg-rich carbonate in ALH 84001. Silicon and trace elements detected by EDS may also reside in residual siderite. Elevated carbon found associated with iron concentrations in the shocked sample is consistent with the magnetite + graphite assemblage described by French (1971) from siderite stability experiments in controlled fO_2 atmospheres. Hematite detected in the siderite starting material could also contribute to magnetite formation according to the equilibrium reaction:

$$\text{carbonate} + \text{hematite} = \text{magnetite} + CO_2$$

for pure siderite and $siderite_{60}magnesite_{40}$ (Koziol 2004). It should be noted that “chemical purity” has not been the sole property of biogenic magnetite since Maher and Taylor (1988) demonstrated that impurity-free magnetite microcrystals with perfect crystal faces only 10–30 nm across are produced pedogenically and can be reproduced in controlled laboratory simulations of pedogenesis.

Local target conditions such as porosity, in this case on the scale of tens of micrometers, are believed to play a large role in pressure (and resulting temperature) excursions that determine whether or not melting or devolatilizations occurs. Original porosity variations could explain the heterogeneous distribution of shock produced nanophase magnetite in siderite interiors. No textural, structural, or compositional evidence for melting was found in siderite shocked to 49 GPa. These are the first experiments to provide information on the earliest stages of incipient shock decomposition in carbonates.

Table 2. D-spacing measurements from SAEDs (Å) of shock experiment products compared to published values for magnetite and magnesioferrite. Within 1% uncertainty in the measurements the d-spacings are indistinguishable.

Intensity	Miller indices	Interplanar spacings for magnetite[a]	Interplanar spacings for magnesioferrite[b, c]	Shocked sample 1	Shocked sample 2	Shocked sample 3
35	220	2.967	2.969	2.97	2.99	2.91
100	311	2.536	2.532	2.48	2.49	2.53
25	400	2.099	2.099	2.11	2.09	2.15
30	511	1.616	1.616	1.62	1.61	1.60
40	440	1.485	1.485	1.48	1.46	1.48

[a]Joint Committee for Powder Diffraction file 19-629.
[b]High temperature form.
[c]Joint Committee for Powder Diffraction file 17-465.

DISCUSSION OF MAGNETITE FORMATION IN ALH 84001

Shock damage in rocks is a function of many material properties including bulk density, porosity, modal mineral compositions, compressibility, and shock impedance variations between adjacent minerals, variations in volatile content, and macroscopic and microscopic structural features. The peak pressure at which specific types of deformation occur (fracturing, plastic deformation, phase transformations, melting, vaporization) is a complex function of material properties coupled with the character of the shock event (Lyzenga et al. 1983; Boslough 1988). The material properties of ALH 84001 include a mixture of phases that vary on the scale of tens of micrometers and include carbonate minerals, each with their own decomposition temperatures. Proponents of magnetite formation as a result of shock metamorphism in ALH 84001 have invoked two scenarios: simple heating (Brearley 2003; Golden et al. 2004) and partial decomposition of siderite and a scenario in which carbonate crystallized from a shock-formed fluid followed by decomposition on cooling (Barber and Scott 2006; Scott et al. 1997).

Brearley (2003) describes carbonate in ALH 84001 as "exhibiting pronounced domainal microstructure, complex strain contrast, and a mottled appearance that is caused by the presence of myriad magnetite crystals and voids" formed by CO_2 loss and draws the conclusion that the carbonate predates the shock event that produced the feldspathic glass. Bradley et al. (1998) also observed voids associated with magnetite in Fe-rich carbonate and that some carbonate rosettes in ALH 84001 are extensively penetrated by networks of feldspathic glass-containing veins. Barber and Scott (2006) observed a carbonate disk that they claim shows no evidence for shock deformation but which exhibits a substructure of elongated, slightly misoriented subcells in the exterior regions, leading them to conclude that the carbonate crystallized from a shock-formed fluid followed by decomposition on cooling. However, the "spectacular zoning" described by Shearer and Adcock (1998) is shown as evidence for carbonate precipitation by non-equilibrium crystallization at low temperature in an open-fracture system and reflects changes in the openness of the hydrothermal system. The precipitation products were then disrupted by a succeeding shock event during which silicate melt detached and shattered many carbonate concretions (Schwandt et al. 1999; Shearer and Adcock 1998) and thermally decomposed the siderite-rich rims to magnetite and associated void space. That the magnetites in ALH 84001 formed by decomposition can be further attested to by the presence of cracks or fractures present where the Fe-rich compositions of the carbonate globules are adjacent to the feldspathic glass. These fractures represent a volume decrease resulting from decomposition leaving a porous aggregate of magnetites and are not present where glass is in contact with less Fe-rich compositions (Brearley 2003; Shearer and Adcock 1998). The magnesite layers show no textural (voids) or compositional (diffusion or depletions) evidence of corrosion effects at their margins (see Brearley 2003, Fig. 13). Finally, Eiler et al. (2002) conclude from oxygen-isotope and trace-element analysis that formation of "carbonate concretions" in ALH 84001 is inconsistent with models involving high-temperature hydrothermal alteration, metamorphism, or carbonate-melt injection. It could be argued that the misoriented subcells in ALH 84001 carbonate described by Barber and Scott are also evidence of deformation during the shock event that mobilized feldspar and decomposed siderite.

Therefore, impact shock metamorphism could provide the thermal input to convert siderite to magnetite in any of several impact events to which ALH 84001 has been subjected (Treiman 1998). The petrological and mineralogical changes induced by impacts, including phase transformations, depend on shock pressure and duration (Duvall and Graham 1977). If ejection is a low-pressure phenomenon (Melosh 1995), how or when could the ALH material be heated to produce magnetite? Possible scenarios for prolonging thermal pulse duration after impact event(s) include insulation in a suevite layer (Bell et al. 1996; Dodd 1981; Simonds 1978) after impact to bring cumulate rock (like ALH 84001) from depth to Mars's surface, or during impact events the material may have suffered before ejection from Mars (Treiman 2003). In the pressure range from 10 to

40 GPa, in experimental shock studies, localized zones of very high temperature have been observed (Lyzenga et al. 1983; Boslough 1988). These observations suggest that shock events in this pressure range produce very intense localized deformation with associated high temperatures even though the bulk temperatures do not increase dramatically. Therefore, shock barometry based on shock-induced reduction of the refractive index in plagioclase feldspar from ALH 84001 may indicate a "bulk" peak pressure of ~32 GPa. However, Barber and Scott (2006) found no evidence of recrystallization or recovery in deformed orthopyroxene crystals in fracture zones in ALH 84001 and concluded that no global heating event occurred in the meteorite. Consequently, the formation of magnetite from decomposed iron carbonate in ALH 84001 must have occurred in the most severe shock event to which it was subjected for local thermal excursions to be great enough to decompose siderite.

The magnetite-rich zone in ALH 84001 is very porous on the nanometer scale (Barber and Scott 2002, 2003). TEM reveals this material to consist of many nanometer-sized magnetite crystals left from the decomposition of siderite—the iron carbonate being a likely component of the natural carbonate precipitation sequence (Golden et al. 2004). If the magnetite in ALH 84001 was allochthonous, there is no reason for the magnetite to be concentrated only in two zones sandwiching the magnesite layer and not distributed throughout the meteorite, or at least distributed throughout the carbonate, given the many pathways created by the numerous deformation events proposed (see Treiman 1998 for a synopsis).

Golden et al. (2004) found that "thermal decomposition of siderite produces magnetite crystals that are identical to those found in ALH 84001" and, more importantly, they found that "most of the purported biogenic magnetite crystals in ALH 84001 do not have the reported [111]-THO morphology, and so are not identical to those from the MV-1 bacterium." Furthermore, Golden et al. (2006) analyzed eleven ALH 84001 magnetites and measured compositions ranging from 100 mol% magnetite to magnetite containing nearly 7 mol% Mg (uncertainties in these measurements are ±0.9 mol%). These observations indicate that ALH 84001 magnetites do not share the characteristics of chemical purity or the [111]-THO crystal morphology with MV-1 bacterium produced magnetites and therefore do not meet the biomarker criterion.

CONCLUSIONS

Only a few things are known about ALH 84001 unequivocally: it is an orthopyroxenite that was formed at depth on a body other than Earth (Clayton 1993; Clayton and Mayeda 1996) (probably Mars) and it contains evidence of shock metamorphism requiring at least 32 GPa (Fritz et al. 2005). Not all of the conditions experienced by ALH 84001 can be replicated by a shock experiment—a natural event of magnitude great enough to excavate material buried several tens of kilometers to the spall zone of an impactor (Shuster and Weiss 2005 and references therein) will produce elevated temperatures of longer duration. However, these shock experiments to 49 GPa decomposed siderite to produce magnetite and so could have achieved temperatures of at least 450 °C to 480 °C. Magnetites produced in these shock experiments display the same range of single-domain sizes (~50–100 nm), compositions (100% magnetite to 80% magnetite-20% magnesioferrite), and morphologies (equant, elongated, euhedral to subhedral) as magnetites synthesized by Golden et al. (2001) and as the magnetites in Martian meteorite ALH 84001. None of these forms of magnetite are a strict match to the magnetite produced by MV-1 bacterium.

In light of these details, shock decomposition of iron carbonate is a reasonable and likely mechanism for magnetite formation in ALH 84001.

Acknowledgments–This work is supported by Lockheed Martin, Jacobs Engineering, and NASA's Cosmochemistry Program. Gerry Hanes performed the shock experiments at Johnson Space Center and his work is appreciated. D. C. Golden is thanked for his help with TEM. Craig Schwandt is thanked for his help with EMP analysis and for valuable critiques. Dick Morris is thanked for the siderite sample and Mossbauer analysis. Stuart Hall provided the magnetic susceptibility measurements and he is thanked. Fred Hörz, Mike Zolensky, Arch Reid, and Doug Ming are thanked for their enlightening discussions which improved this paper immensely. Detailed and useful reviews by E. R. D. Scott, D. Barber, and two anonymous reviewers are gratefully acknowledged.

Editorial Handling—Dr. Edward Scott

REFERENCES

Bagin V. I. and Rybak R. S.1970. The decomposition of siderite by heat. *Bulletin of the Academy of Science USSR* 6:395–398.

Baker P. A. and Burns S. J. 1985. Occurrence and formation of dolomite in organic-rich continental margin sediments. *AAPG Bulletin* 69:1917–1930.

Barber D. J. and Scott E. R. D. 2003. Transmission electron microscopy of minerals in the Martian meteorite ALH 84001. *Meteoritics & Planetary Science* 38:831–848.

Barber D. J. and Scott E. R. D. 2006. Shock and thermal history of Martian meteorite Allan Hills 84001 from transmission electron microscopy. *Meteoritics & Planetary Science* 41:643–662.

Bell M. S., Reagan M. K., Anderson R. R., and Foster C. T. 1996. Petrology of the crystalline clast breccias from the Manson M-1 core. In *The Manson impact structure, Iowa: Anatomy of a crater*, edited by Koeberl C. and Anderson R. R. GSA Special Paper #302. Boulder, Colorado: Geological Society of America. pp. 221–234.

Bell M. S., Thomas-Keprta K. L., Wentworth S. J., and McKay D. S. 1999. Microanalysis of pyroxene, feldspar, and silica glass in

Allan Hills 84001 (abstract). *Meteoritics & Planetary Science* 34:A10.

Bell M. S., Lin I.-C., and McKay D. S. 2000. Analysis of siderite decomposition by differential scanning calorimetry. In *Catastrophic events and mass extinctions: Impacts and beyond*, edited by Koeberl C. and MacLeod K. G. GSA Special Paper #1053. Boulder, Colorado: Geological Society of America. pp. 8–9.

Bell M. S., Schwandt C., Zolensky M. E., and Hörz F. 2002. Experimental shock decomposition of siderite (abstract). *Meteoritics & Planetary Science* 37:A14.

Boslough M. B. 1988. Post-shock temperatures in silica. *Journal of Geophysical Research B* 93:6477–6484.

Bradley J. P., McSween H. Y., Jr., and Harvey R. P. 1998. Epitaxial growth of nanophase magnetite in Martian meteorite Allan Hills 84001: Implications for biogenic mineralization. *Meteoritics & Planetary Science* 33:765–773.

Brearley A. J. 1986. An electron optical study of muscovite breakdown in peletic xenoliths during pyrometamorphism. *Mineralogical Magazine* 50:385–397.

Brearley A. J. 2003. Magnetite in ALH 84001: An origin by shock-induced thermal decomposition of iron carbonate. *Meteoritics & Planetary Science* 38:849–870.

Clayton R. N. and Mayeda T. K. 1996. Oxygen isotope studies of achondrites. *Geochimica et Cosmochimica Acta* 60:1999–2017.

Criado J. M., Gonzalez M., and Macias M. 1988. Influence of grinding on both the stability and thermal decomposition mechanism of siderite. *Thermochimica Acta* 135:219–223.

Deer W. A., Howie R. A., and Zussman J. 1997. *An introduction to the rock-forming minerals*. Harlow: Addison Wesley Longman Limited. 696 p.

Dodd R. T. 1981. *Meteorites: A petrologic-chemical synthesis*. Cambridge: Cambridge University Press. 368 p.

Duvall G. E. and Graham R. A. 1977. Phase transformations under shock-wave loading. *Reviews of Modern Physics* 49:523–579.

Eiler J. M., Valley J. W., Graham C. M., and Fournelle J. 2002. Two populations of carbonate in ALH 84001: Geochemical evidence for discrimination and genesis. *Geochimica et Cosmochimica Acta* 66:1285–1303.

Ellwood B. B., Chrzanowski T. J., Long G. J., and Buhl M. L. 1988. Siderite formation in anoxic deep-sea sediments: A synergistic bacterially controlled process with important implications in paleomagnetism. *Geology* 16:980–982.

French B. M. 1971. Stability relations of siderite ($FeCO_3$) in the system Fe-C-O. *American Journal of Science* 271:37–78.

Fritz J., Artemieva N., and Greshake L. 2005. Ejection of Martian meteorites. *Meteoritics & Planetary Science* 40:1393–1411.

Gallagher P. K. and Warne S. S. J. 1981. Thermomagnetrometry and thermal decomposition of siderite. *Thermochimica Acta* 43:263–267.

Gibbons R. V., Hörz F., Thompson T. D., and Ahrens T. J. 1975. Controlled shock experiments of lunar analogues. In *Lunar Science VI*. Houston, Texas: Lunar Science Institute. pp. 284–286.

Golden D. C., Ming D. W., Lauer H. V., Jr., Morris R. V., Treiman A. H., and McKay G. A. 2006. Formation of "chemically pure" magnetite from Mg-Fe-carbonates: Implications for the exclusively inorganic origin of magnetite and sulfides in Martian meteorite ALH 84001 (abstract #1199). 37th Lunar and Planetary Science Conference. CD-ROM.

Golden D. C., Ming D. W., Schwandt C. S., Lauer H. V., Jr., Socki R. A., Morris R. V., Lofgren G. E., and McKay G. A. 2001. A simple inorganic process for formation of carbonates, magnetite, and sulfides in Martian meteorite ALH 84001. *American Mineralogist* 86:370–375.

Golden D. C., Ming D. W., Morris R., Brearley A. J., Lauer H. V., Jr., Treiman A. H., Zolensky M. E., Schwandt C. S., Lofgren G. E., and McKay G. A. 2004. Evidence for exclusively inorganic formation of magnetite in Martian meteorite ALH 84001. *American Mineralogist* 89:681–695.

Harker R. I. and Tuttle O. F. 1955. Studies in the system CaO-MgO-CO_2: Part 1. The thermal dissociation of calcite, dolomite, and magnesite. *American Journal of Science* 253:209–224.

Heinrich K. F. J. 1981. *Electron beam and X-ray microanalysis*. New York: Van Nostrand Reinhold Co. 578 p.

Hörz F. 1970. A small ballistic range for impact metamorphism studies. NASA Technical Note #TN D-5787. 16 p.

Joint Committee on Powder Diffraction Standards. 1980. *Mineral powder diffraction file: Data book*. Swarthmore, Pennsylvania: JCPDS International Center for Diffraction Data. 1168 p.

Koziol A. M. 2004. Experimental determination of siderite stability and application to Martian meteorite ALH 84001. *American Mineralogist* 89:294–300.

Koziol A. M. and Newton R. C. 1995. Experimental determination of the reactions magnesite + quartz = enstatite + CO_2 and magnesite = periclase + CO_2, and the enthalpies of formation of enstatite and magnesite. *American Mineralogist* 80:1252–1260.

Kulp J. L., Kent P., and Kerr P. F. 1951. Thermal study of the Ca-Mg-Fe carbonate minerals. *American Mineralogist* 36:643–670.

Langenhorst F., Shaw C. S. J., and Metzler K. 2000. Mineral chemistry and microstructures in ALH 84001 (abstract #1866). 31st Lunar and Planetary Science Conference. CD-ROM.

Lin I.-C., Lauer H. V., Jr., Golden D. C., and Ming D. W. 2000. Differential scanning calorimetry of volatile-bearing iron minerals under Mars-like pressures: New insights into energetics and mechanisms of thermal decomposition. (abstract #1417). 31st Lunar and Planetary Science Conference. CD-ROM.

Lyzenga G. A., Ahrens T. J., and Mitchell A. C. 1983. Shock temperatures of SiO_2 and their geophysical implications. *Journal of Geophysical Research B* 88:2431–2444.

Maher B. A. and Taylor R. M. 1988. Formation of ultrafine-grained magnetite in soils. *Nature* 336:368–370.

McKay D. S., Gibson E. K., Jr., Thomas K. K. L., Vali H., Romanek C. S., Clemett S. J., Chillier X. D. F., Maechling C. R., and Zare R. N. 1996. Search for past life on Mars: Possible relic biogenic activity in Martian meteorite ALH 84001. *Science* 273:924–930.

Melosh H. J. 1995. Cratering dynamics and the delivery of meteorites to the Earth. *Meteoritics & Planetary Science* 30:545–546.

Mittlefehldt D. W. 1994. ALH 84001, a cumulate orthopyroxenite member of the Martian meteorite clan. *Meteoritics* 29:214–221.

Nickel E. H. 1992. Solid solutions in mineral nomenclature. *Canadian Mineralogist* 30:231–234.

Nickel E. H. and Grice J. D. 1998. The IMA commission on new minerals and mineral names: Procedures and guidelines on mineral nomenclature. *Canadian Mineralogist* 36:913–926.

Osinski G. R. and Spray J. G. 2001. Impact-generated carbonate melts: Evidence from the Haughton structure, Canada. *Earth and Planetary Science Letters* 194:17–29.

Pan Y., Zhu R., Bannerjee S., Gill J., and Williams Q. 2000. Rock magnetic properties related to thermal treatment of siderite: Behavior and interpretation. *Journal of Geophysical Research* 105:783–794.

Ranganthan V. and Tye R. S. 1986. Petrography, diagenesis, and facies controls on porosity in Shannon Sandstone, Hartzog Draw Field, Wyoming. *AAPG Bulletin* 70:56–60.

Schaller W. T. 1930. Adjectival ending of chemical elements used as modifiers to mineral names. *American Mineralogist* 15:567–574.

Schwandt C. S., McKay G. A., and Lofgren G. E. 1999a. FESEM imaging reveals previously unseen detail and enhances interpretations of ALH 84001 carbonate petrogenesis (abstract

#1346). 30th Lunar and Planetary Science Conference. CD-ROM.

Schwandt C. S., McKay G. A., and Lofgren G. E. 1999b. Silica in Martian meteorites, there are differences (abstract #1637). 30th Lunar and Planetary Science Conference. CD-ROM.

Scott E. R. D. and Barber D. J. 2002. Origin of magnetite in Martian meteorite Allan Hills 84001 (abstract). *Meteoritics & Planetary Science* 37:A128.

Scott E. R. D., Yamaguchi A., and Krot A. N. 1997. Petrological evidence for shock melting of carbonates in the Martian meteorite ALH 84001. *Nature* 387:377–379.

Shearer C. K. and Adcock C. T. 1998. The composition and distribution of feldspathic shock glass in ALH 84001 (abstract #1280). 29th Lunar and Planetary Science Conference. CD-ROM.

Simonds C. H., Floran R. J., McGee P. E., Phinney W. C., and Warner J. L. 1978. Petrogenesis of melt rocks, Manicouagan impact structure, Quebec. *Journal of Geophysical Research* 83:2773–2788.

Stöffler D. 2000. Maskelynite confirmed as diaplectic glass: Indication for peak shock pressures below 45 GPa in all Martian meteorites. (abstract #1170). 31st Lunar and Planetary Science Conference. CD-ROM.

Telford W. M., Geldart L. P., Sherriff R. E., and Keys D. A. 1976. *Applied geophysics*. Cambridge: Cambridge University Press. 121 p.

Thomas-Keprta K. L., Bazylinski D., Kirschvink J. L., Clemett S. J., McKay D. S., Wentworth S. J., Vali H., Golden D. C., Gibson E. K., and Romanek C. S. 2000. Elongated prismatic magnetite crystals in ALH 84001 carbonate globules: Potential Martian magnetofossils. *Geochimica et Cosmochimica Acta* 64:4049–4081.

Thomas-Keprta K. L., Clemett S. J., Bazylinski D., Kirschvink J. L., McKay D. S., Wentworth S. J., Gibson E. K., McKay M. F., and Romanek C. S. 2001. Truncated hexa-octahedral magnetite crystals in ALH 84001: Presumptive biosignatures. *Proceedings of the National Academy of Sciences* 98:2164–2169.

Thomas-Keprta K. L., Clemett S. J., Bazylinski D. A., Kirschvink J. L., McKay D. S., Wentworth S. J., Vali H., Gibson E. K., and Romanek C. S. 2002. Magnetofossils from ancient Mars: A robust biosignature in the Martian meteorite ALH 84001. *Applied and Environmental Microbiology* 68:3663–3672.

Treiman A. 1998. The history of ALH 84001 revised: Multiple shock events. *Meteoritics & Planetary Science* 33:753–764.

Treiman A. H. 2003. Submicron magnetite grains and carbon compounds in Martian meteorite ALH 84001: Inorganic, abiotic formation by shock and thermal metamorphism. *Astrobiology* 3: 369–392.

Shuster D. L. and Weiss B. P. 2005. Martian surface paleotemperatures from thermochronology of meteorites. *Science* 309:594–597.

Zakharov V. Y. and Adonyi Z. 1986. Thermal decomposition kinetics of siderite. *Thermochimica Acta* 102:101–107.